

Dual-function RNA-binding proteins influence mRNA abundance and translational efficiency of distinct sets of target genes

Valentin Schneider-Lunitz^{1,§}, Jorge Ruiz-Orera^{1,§}, Norbert Hubner^{1,2,3,*}, Sebastiaan van Heesch^{4,*}

¹Cardiovascular and Metabolic Sciences, Max Delbrück Center for Molecular Medicine in the Helmholtz Association (MDC), 13125 Berlin, Germany

²DZHK (German Centre for Cardiovascular Research), Partner Site Berlin, 13347 Berlin, Germany.

³Charité-Universitätsmedizin, 10117 Berlin, Germany.

⁴The Princess Máxima Center for Pediatric Oncology, Heidelberglaan 25, 3584 CT Utrecht, Utrecht, The Netherlands.

§These authors contributed equally

*Correspondence: S.vanHeesch@prinsesmaximacentrum.nl and nhuebner@mdc-berlin.de

Keywords

RBP; dual-function; translational efficiency; ribosome profiling; Ribo-seq; heart; translational regulation; CLIP-seq

ABSTRACT

RNA-binding proteins (RBPs) are key regulators of RNA metabolism. Many RBPs possess uncharacterized RNA-binding domains and localize to multiple subcellular compartments, suggesting their involvement in multiple biological processes. We searched for such multifunctionality within a set of 143 RBPs by integrating experimentally validated target genes with the transcriptomes and translomes of 80 human hearts. This revealed that RBP abundance is predictive of the extent of target regulation *in vivo*, leading us to newly associate 27 RBPs with translational control. Amongst those were several splicing factors, of which the muscle specific RBM20 modulated target translation rates through switches in isoform production. For 21 RBPs, we newly observed dual regulatory effects impacting both mRNA levels and translation rates, albeit for virtually independent sets of target genes. We highlight a subset, including G3BP1, PUM1, UCHL5, and DDX3X, where dual regulation is achieved by differential affinity for targets of distinct length and functionality. Strikingly, in a manner very similar to DDX3X, the known splicing factors EFTUD2 and PRPF8 selectively influence target translation rates depending on 5' UTR structure. Our results indicate unanticipated complexity of protein-RNA interactions at consecutive stages of gene expression and implicate multiple core splicing factors as key regulators of translational output.

INTRODUCTION

RNA-protein interactions are crucial for a wide range of processes across subcellular compartments, including RNA transcription, splicing, editing, transport, stability, localization, and translation (Gerstberger et al., 2014). Using state-of-the-art mass spectrometry-based approaches, recent studies have identified up to thousands of potential RNA-binding proteins (RBPs), although for many their precise roles remain unknown (Caudron-Herger et al., 2019; Mallam et al., 2019; Trendel et al., 2019). Whereas many of these RBPs interact with

target RNAs through well-defined protein-RNA binding domains (RBD), uncharacterized RBDs are frequently discovered (Castello et al., 2016; Beckmann et al., 2016) highlighting the complex, diverse, and still largely unknown nature of RNA-protein interactions. The possession of more than a single RBD would theoretically allow RBPs to be multifunctional, for instance through the separate regulation of different sets of targets (Kong et al., 2019). Multifunctionality may additionally be established through the condition- or cell type-specific expression of RBPs and their interaction partners, or through dynamic shuttling of RBPs between different cell compartments, such as the nucleus and cytosol (Dassi, 2017; Díaz-Muñoz & Turner, 2018; Gray et al., 2015; Yugami et al., 2020). Accordingly, out of a large number of RBPs for which subcellular localization was recently evaluated (Van Nostrand et al., 2020), the vast majority could be detected in more than one compartment, albeit of thus far largely unknown biological significance. The potential importance of RBP re-localization was exemplified by the subcellular redistribution of dozens of RBPs upon global induction of mRNA decay (Gilbertson et al., 2018), or the compartment-specific changes in RBP interactomes that can be witnessed upon cellular stress (Backlund et al., 2020). Both observations indicate that RBPs may either be temporarily kept in a compartment where they are not functional, or, in contrast, use their dynamic ability to relocate to form a mechanistic bridge between normally compartment-restricted consecutive stages of gene expression regulation: some taking place in the nucleus (e.g., transcription, mRNA processing, splicing), others in the cytosol (e.g., translation, RNA decay).

In the cytosol, RBPs are crucial regulators of mRNA translation - the synthesis of protein from a messenger RNA template by ribosomes (Hinnebusch, 2014). During translation, RBPs can act in a general capacity (e.g., mRNA translation initiation or elongation), as well as in more specialized functions where select accessory RBPs or heterogeneous ribosomes facilitate the translation of dedicated subsets of target RNAs (Harvey et al., 2018; Shi et al., 2017; Simsek et al., 2017). Mechanistic insight into the quantitative effects of RBP expression on mRNA translation - i.e., when translation rates of the endogenous RBP targets respond directly to changes in RBP levels -

was recently provided by several studies that used this relationship to assign novel functions to known RBPs (Chothani et al., 2019; Luo et al., 2020; Sharma et al., 2021) and to define the kinetics through which RBPs regulate their targets (Sharma et al., 2021). Chothani *et al.* used a correlation-based approach, for which the frequency with which RBP levels correlate with target translation rates was used to pinpoint key RBP network hubs crucial for translational regulation during cardiac fibrosis (Chothani et al., 2019). In a separate study, Luo *et al.* used luciferase-based 3' UTR tethered function assays for 690 RBPs and identified 50 RBPs whose expression induced significant positive or negative effects on mRNA stability and/or translation. This resulted in the novel identification of the stress granule RBP UBAP2L as a ribosome-associated RBP (Luo et al., 2020). Lastly, Sharma *et al.* developed a new approach to investigate RNA-protein kinetics in a time-resolved manner for the RBP DAZL (Sharma et al., 2021). This technique helped establishing a quantitative relationship that explains the effect of DAZL on mRNA levels and ribosome association, which appeared to correlate with the cumulative probability of DAZL binding within clusters of proximal 3' UTR binding sites. However, whether such quantitative relationships between RBPs and their targets exist *in vivo*, and thereby impact the extent of translational control by RBPs in human tissues, has not been investigated.

Here, we describe the identification of RBPs with more than a single function in the human heart – a tissue where translational control is known to play a central role in gene expression regulation (Chothani et al., 2019; Van Heesch et al., 2019; Schafer et al., 2015b). Integrating crosslinking immunoprecipitation (CLIP)-derived mRNA targets for 143 RBPs (Van Nostrand et al., 2020; Maatz et al., 2014) with the transcriptomes and translomes of 80 human hearts (Van Heesch et al., 2019), we could show that the expression levels of many, but not all, investigated RBPs correlated with target mRNA abundance and/or translational efficiency *in vivo*. Based on these observations we implicated 37 out of 143 RBPs to function in translational regulation, of which 27 were not known to be involved in translational control before. Amongst those 27 RBPs were multiple key splicing regulators, such as the muscle-specific splicing factor RBM20, which appeared to influence protein synthesis through changes in transcript isoform production ratios. Of note, for a subset of 21 RBPs (including G3BP1, DDX3X, PUM1, and UCHL5), we could independently assign dose-dependent effects to both mRNA levels and translational efficiencies of largely distinct sets of target genes involved in unrelated biological processes. Mechanistically, these target genes also appeared to be regulated independently, facilitated by a differential affinity for coding sequence length or 5' UTR structure, but not through alterations in the RNA binding motifs that were being recognized. A key observation is the highly similar and specific behavior observed for DDX3X, as well as the known splicing factors EFTUD2 and PRFP8 – all three recognized as dual-function RBPs by our analysis – in regulating the translational output of targets in a manner that depends on the structure of the target's 5' UTR.

Our results show that RBPs with dual roles are more prevalent than currently anticipated and seemingly couple multiple splicing factors to translational control. We postulate that dual-function RBPs may use their functional plasticity in a condition- or compartment-specific manner to fine-tune the expression of distinct sets of target genes.

RESULTS

RNA-binding protein abundance determines the efficiency of target gene translation

To determine whether RBP abundance has predictive value for the extent of target gene regulation in human tissue, we compiled and reanalyzed protein-RNA interactions for a set of 143 cardiac-expressed RBPs, consisting of the muscle-specific RBM20 (Maatz et al., 2014) and 142 ubiquitously expressed RBPs (Van Nostrand et al., 2020) (see Methods and **Figure S1A**). We then correlated the abundance of these 143 RBPs with the translational efficiency (TE) of 11,387 cardiac-expressed genes across all 80 human hearts (Van Heesch et al., 2019). This revealed a quantitative dependency between the expression level of the RBP and the extent of target gene translational control (**Figure 1A** and **Figure S1B**). Next, we calculated the frequency with which the mRNA levels and translational efficiencies of known CLIP-derived target genes correlated significantly with the abundance of each RBP. We statistically evaluated these associations through the sampling of 100,000 matched sets of simulated target genes, yielding significant associations (empirical $p_{\text{adj}} \leq 0.05$) for 58 RBPs with target mRNA abundance (hereafter denoted as “mRNA-RBPs” that regulate “mRNA targets”) and 37 RBPs with target translational efficiency (“TE-RBPs” regulating “TE targets”) (**Figure 1B** and **Figure S1C**). These for instance include the candidate tumor suppressor and splicing regulator RBM5, which we identify as an mRNA-RBP (138 correlating targets; $p_{\text{adj}} = 2.83 \times 10^{-5}$; Glass' $\Delta = 27.2$) (Sutherland et al., 2010). Also, expression dynamics of the TE-RBP EIF4G2 correspond with target gene translational efficiencies (235 correlating targets; $p_{\text{adj}} = 5.26 \times 10^{-5}$; Glass' $\Delta = 6.3$), matching its function as a non-canonical translation initiation factor (Lieberman et al., 2009; Weber R, Kleemann L, Hirschberg I, Chung M, Valkov E, 2021) (**Figure 1B**). Reassuringly, for 25 out of 37 potential TE-RBPs we could replicate our observations in an independent, though smaller cohort of primary cardiac fibroblast translomes ($n = 20$; (Chothani et al., 2019)) (**Figure 1C**).

Positive and negative control of translation by known and unknown factors

In order to identify RBPs that coordinately regulate target gene translation, we hierarchically clustered the correlation coefficients of the 37 TE-RBPs and their CLIP targets. This divided the TE-RBPs into two distinct groups with marked opposite effects on TE, indicative of competition and/or cooperation between RBPs (**Figure 2A**). For different groups of shared targets, we could identify TE-RBP clusters with opposite or concordant directionality of regulation depending on the RBP (**Figure 2B**). For instance, depending on the shared target gene that is bound by two selected TE-RBPs - e.g., the splicing factor U2AF2 and the protease UCHL5 - completely opposite effects on TE can be observed and independently replicated (**Figure 2B**, **S2A** and **S2B**). Although these shared modes of target regulation are in part concordant with protein-protein interactions annotated in the STRING database (39), a subset of coregulatory “RBP hubs” contain proteins with previously unknown functional similarities (e.g., UCHL5 and U2AF2).

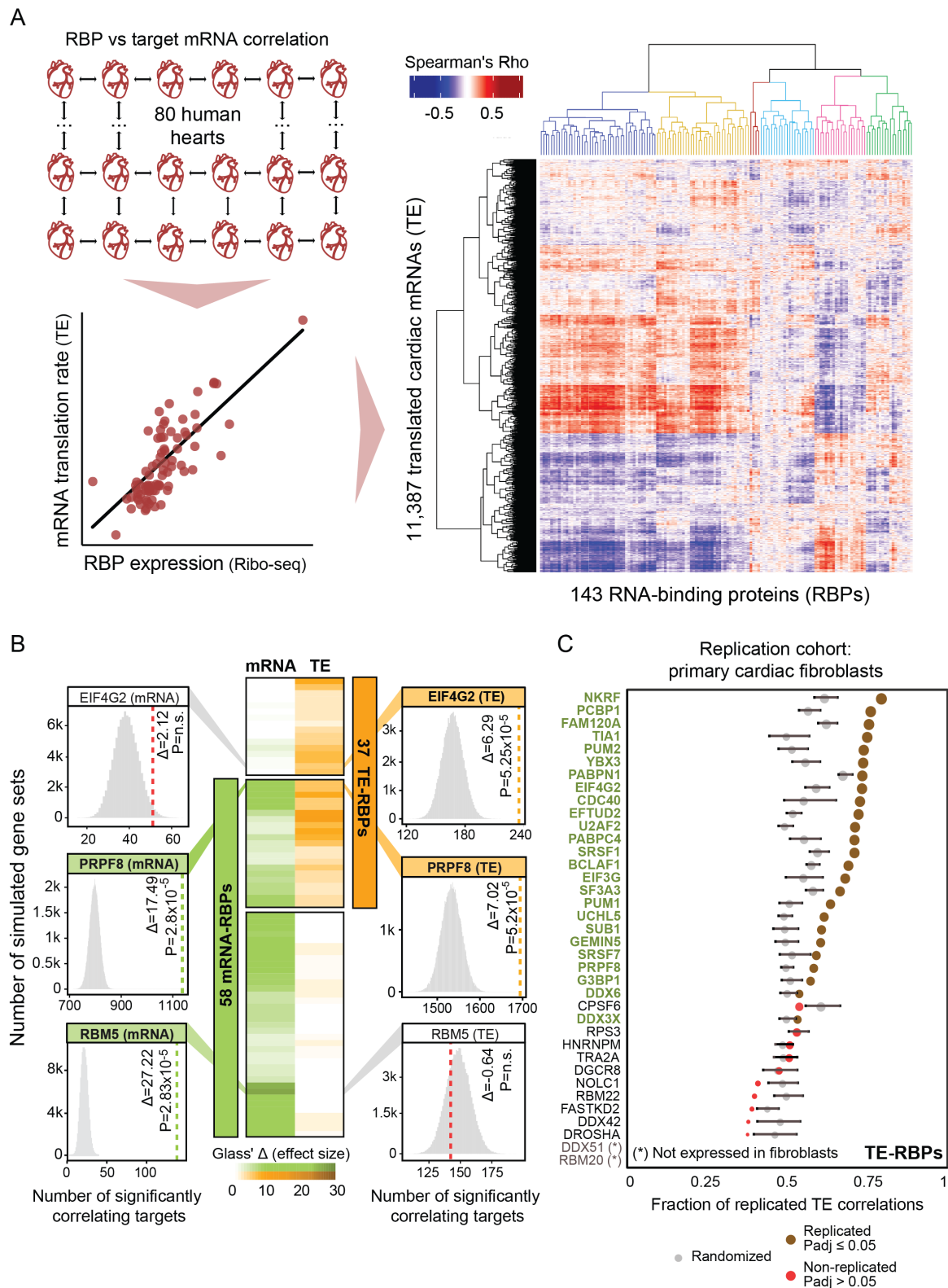


Figure 1. RNA-binding protein abundance predicts target translational regulation. (A) Schematic of the RBP-target correlation approach. Using the quantified Ribo-seq and RNA-seq data from 80 hearts, pairwise RBP versus target mRNA abundance or translational efficiency correlations were calculated. A heatmap with hierarchically clustered translational efficiency Spearman's Rho correlations of RBPs and translated mRNAs in the human heart are shown. Six clusters of coregulated RBPs are highlighted (See also **Table S1**). (B) Heatmap with Glass' Δ scores that quantify the effect size of the witnessed significance of associations between RBPs and target gene mRNA abundance and TE. Only significant RBPs are shown: 37 TE-RBPs (orange) and 58 mRNA-RBPs (green). For three selected RBPs (one per category), histograms illustrate the significance of the calculated associations. (C) Dot plot displaying the fraction of translational efficiency RBP-target correlations that can be replicated in an independent set of primary cardiac fibroblasts (Chothani *et al.* 2019). For each RBP, the significance of the replication was evaluated by comparing the replicated fraction between observed and randomized sets and it is represented as a brown (significant) or red (non-significant) dot. The size of the dots indicates the strength of significance ($-\log_{10}(p_{adj})$) and grey dots correspond to the fraction of replicated correlations in randomized sets. Error bars indicate mean values with standard deviation (SD).

This suggests that these RBPs may be previously missed interaction partners of existing protein-protein networks for the coordinated translational control of a subset of target genes.

To define potential master regulators amongst the 37 TE-RBPs, and thus depict hierarchy within the way these RBPs orchestrate translation, we generated a weighted topological network overlap (wTO, (Gysi et al., 2018; Nowick et al., 2009); see methods). This put 5 out of 37 TE-RBPs, including four splicing factors (HNRNPM, EFTUD2, U2AF2, SF3A3) and a ribosomal protein (RPS3), upstream of most other TE-RBPs (**Figure S2C**). Of the defined five potential master regulators, only RPS3 (Dong et al., 2017) and HNRNPM (Ainaoui et al., 2015; Chen et al., 2019) have previously been implicated in translational regulation. The high number of splicing regulators amongst the TE-RBPs (14 out of 37; 38%) could be considered surprising, though these numbers match the distribution of RBP functions in the initial set of RBPs (49 splicing RBPs out of 143 included RBPs; 34%) (**Figure S2D**). Our results suggest that, through mechanisms yet unknown, multiple ubiquitously expressed splicing factors can have a quantitative impact on protein synthesis. This effect may either be established fully independent of the splicing machinery or be secondary consequence of the qualitative decision of which mRNA isoforms are being produced.

RBM20-directed isoform production influences downstream translational efficiency

In addition to the aforementioned set of splicing factors, we detected more TE-RBPs without prior evidence of regulating mRNA translation: 27 out of 37 TE-RBPs had previously not been implicated in a translation-related process, including 4 RBPs with no function assigned to their RNA binding ability at all (NKRF, FAM120A, SUB1 and UCHL5) (**Figure S2D**). Amongst the 27 new TE-RBPs was also the splicing regulator RBM20, whose expression correlated particularly well with the TE of 163 experimentally validated target genes (out of 561 total targets; Glass' $\Delta = 7.0$; **Figure 2C**).

Importantly, RBM20 levels specifically influenced TE and had no impact on overall mRNA abundance or stability. Most RBM20 targets, including the sarcomere genes *TTN* and *TNNI3K*, correlated positively (i.e., higher RBM20 expression associates with increased target gene TE; **Figure 2D**) and especially those positively correlating targets showed strong enrichment for muscle function processes (GO:0003012, $p_{\text{adj}} \leq 5.97 \times 10^{-16}$) (**Figure 2C**). To investigate a possible connection between RBM20-mediated mRNA splicing and the subsequent efficiency of mRNA translation, we evaluated whether splicing rates of known target exons correlated directly with TE. For 66 out of 163 ($\pm 40\%$) translationally regulated RBM20 target genes, the extent of alternative splicing (PSI; see methods) indeed correlated with RBM20 abundance. A clear example is the exon inclusion measured across the *TTN* I-band, whose exons are only included in the longer *TTN* N2BA isoform. These I-band exons specifically drive the negative correlation of RBM20 expression with overall *TTN* TE, indicating that their inclusion reduces the efficiency with which *TTN* can be translated. We had previously observed that *TTN* translation rates are strongly

isoform-dependent (Van Heesch et al., 2019) and can now mechanistically connect this to splicing control by RBM20 (**Figure 2E**), a consequence that seems generalizable for more muscle-specific RBM20 targets, including other sarcomere components (**Figure 2C+D**). These findings could suggest that variations in the abundance of splicing regulators may mediate protein synthesis rates by defining which isoform is produced. Although the precise mechanism through which RBM20 influences TE remains unknown, this RBP may omit the inclusion of exons with inefficient codon translation rates or exons that impact the stability or structure of the transcript, both of which influence protein synthesis rates (Nott et al., 2004; Zhou et al., 2016).

Dual-function RBPs like DDX3X and G3BP1 regulate mRNA abundance and translational efficiency of independent sets of target genes

Among the 74 RBPs that correlated significantly with target gene TE (37 TE-RBPs) or mRNA abundance (58 mRNA-RBPs), a subset of 21 RBPs could be associated independently with both of these molecular traits (**Figure 1B and 3A**). To investigate whether the association with mRNA abundance and TE was interrelated (and hence successive, i.e., higher target expression drives increased TE), we investigated the sets of genes that correlated significantly with either trait. This revealed a very limited overlap between correlating target genes for all 21 RBPs ($16.71 \pm 8.19\%$, **Figure 3A and Table S2**), which decreased further for the most strongly correlating targets ($1.09 \pm 1.49\%$; $r > 0.5$; **Figure S3A**). To substantiate this observation, we compared the trait-specific strength of the effect sizes and found no relation between the correlations as independently witnessed for both traits, confirming the absence of a carryover effect (**Figure 3B and Figure S3A**). This led us to denote these RBPs as “dual-function RBPs” - context-specific RBPs whose functional outcome depends on the set of mRNAs it targets. A key example appears to be the multifunctional RBP DDX3X (Mo et al., 2021; Soto-Rifo et al., 2012), whose abundance correlates significantly with the mRNA levels of 339 target genes ($p_{\text{adj}} = 2.83 \times 10^{-5}$; Glass' $\Delta = 6.9$) and the translational efficiency of 730 target genes ($p_{\text{adj}} = 5.25 \times 10^{-5}$; Glass' $\Delta = 11.89$), of which only 43 targets overlap between both sets (**Figure 3A-C**). The consequences of DDX3X binding for mRNA abundance (positive correlation) or TE (negative correlation) are opposite, though this is not the case for all dual-function RBPs (**Figure S3B**). Three other dual-function RBPs similarly act as repressors of translation whilst having a positive effect on mRNA abundance (DDX6, NKRF, GEMIN5), one RBP shows the exact opposite behavior (FAM120A), and all others have concordant roles at both layers of control (e.g., TRA2A, FASTKD2, SRSF1).

Of note, the TE and mRNA target genes of dual-function RBPs can be enriched for completely separate biological processes, indicating that duality can contribute to independent biological outcomes. For instance, correlating DDX3X and UCHL5 TE targets code for proteins involved in RNA splicing (GO:0008380, $p_{\text{adj}} = 7.70 \times 10^{-30}$), while their mRNA targets did not show any clear functional enrichment (**Figure 3C**).

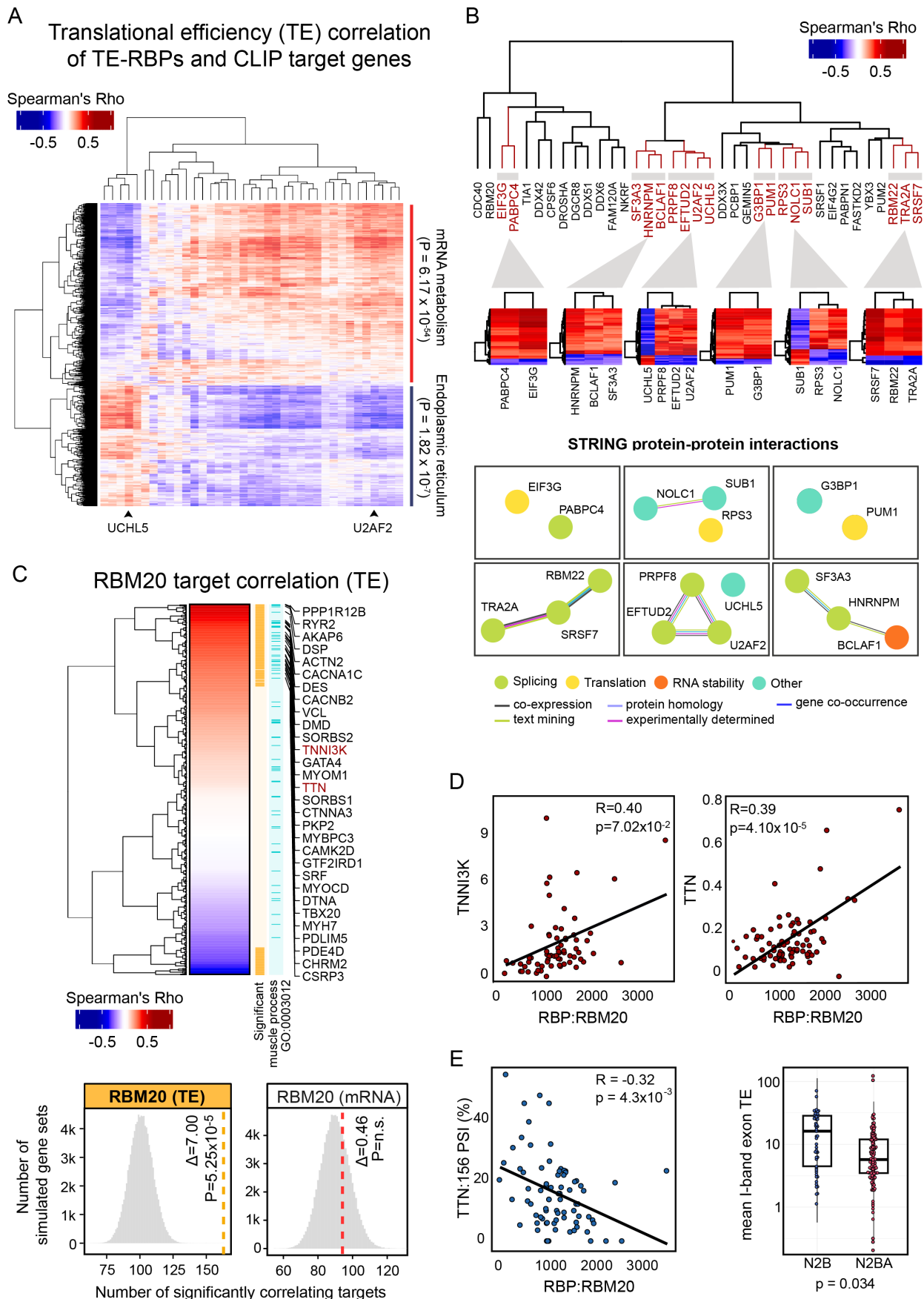


Figure 2. CLIP analysis identifies coregulated *in vivo* targets and novel master translational regulators in the human heart. (A) Heatmap with hierarchically clustered translational efficiency correlations of TE-RBPs and predicted target genes in the human heart is represented. The clustering separates two groups with opposite effects on TE whose targets are enriched in mRNA metabolism ($p_{adj} = 6.17 \times 10^{-54}$) and endoplasmic reticulum ($p_{adj} = 1.82 \times 10^{-7}$) GO terms respectively. **(B)** Dendrogram with hierarchically

clustered TE-RBPs based on pairwise RBP-RBP overlaps. Shared target genes of all paired RBPs were included for clustering. Bottom heatmaps with translational efficiency correlations of selected RBP clusters and shared significant targets. These plots illustrate distinct cooperative and competitive RBP-target regulation modes. STRING protein-protein interaction networks (Szkarczyk *et al.* 2019) from selected RBP clusters reveal functional association of coregulated RBPs. Colours in edges and nodes indicate the sources of STRING evidence and known RBP functions. **(C)** Heatmap with hierarchically clustered Spearman's Rho correlation scores of RBM20 and the translational efficiency of the predicted target genes. Significant correlating targets ($n = 163$, $p_{\text{adj}} \leq 0.05$) and targets involved in muscle process (GO: 0003012) are highlighted in orange and light blue colours respectively. A list of sarcomere gene targets positively correlating with RBM20 is displayed. Selected bottom histograms illustrate the significance of RBM20 with correlating TE targets and the absence of significance with correlating mRNA targets. **(D)** Scatter plots representing the correlation of translational efficiencies between RBM20 and two sarcomere genes, *TNNI3K* and *TTN*. Score and level of significance of the two Spearman's correlations are displayed. **(E)** Left: Scatter plot showing correlation between RBM20 and *TTN* exon:156 percent spliced in (PSI). Score and level of significance of the two Spearman's correlations are displayed. Right: Box plot comparing average *TTN* I-Band isoform-specific TEs. N2B (ENST00000460472) has a significantly higher TE than N2BA (ENST00000591111) (Wilcoxon Rank Sum test: p -value = 0.034).

For G3BP1, mRNA targets code for proteins involved in localization to nuclear body (GO:1903405, $p_{\text{adj}} = 5.13 \times 10^{-12}$), whereas this is not the case for translationally regulated targets, which are enriched for RNA splicing (GO:0008380, $p_{\text{adj}} = 1.61 \times 10^{-10}$). Such biological discrepancies are not always present: independent of the mode of regulation, both types of PUM1 targets (TE or mRNA) appear to code for proteins involved in mRNA processing (GO:0006397, TE $p_{\text{adj}} = 2.64 \times 10^{-22}$, mRNA $p_{\text{adj}} = 6.40 \times 10^{-13}$).

Differential affinity of dual-function RBPs for CDS lengths and 5' UTR structures

Dual- or multiprotein functionality can be achieved through context-specific differences in subcellular localization (Buchan, 2014), interaction partners (Cirillo *et al.*, 2020; Yang *et al.*, 2019), or the presence of multiple RNA-binding domains (Müller-McNicoll & Neugebauer, 2013) - all of which can finetune or restrict the subset of recognized target genes. Based on published immunofluorescence imaging-based evidence of subcellular RBP localization (Van Nostrand *et al.*, 2020), 13 out of 21 dual-function RBPs indeed localized equally well to both nucleus and cytosol, suggesting functionality in both compartments (**Table S3**). We further examined the spatial patterns of binding motifs on target genes for three dual-function RBPs with catalogued motif data (U2AF2, PUM1, TRA2A (Benoit Bouvrette *et al.*, 2020)). The frequency and inter-site distance of these RBP motifs was similar for TE and mRNA targets, indicating that dual-function RBPs likely recognize similar RNA-binding motifs to regulate the abundance and translation of independent groups of mRNAs.

We additionally explored the relative position of CLIP binding sites in target genes (i.e., the position of binding within the mRNA: 5' UTR, CDS, 3' UTR or intronic). Most of the RBPs (including e.g., DDX3X) showed no marked difference in binding positioning (**Figure S3B**). For DDX3X and 10 other RBPs, we did notice a significant change in target transcript length, mostly explained by differences in target CDS length, which slightly increased or decreased between TE and mRNA targets (**Figure 3D** and **S3C**). The most significant changes in CDS length were seen for GEMIN5 (decrease for TE targets; 2,226nt vs. 1,519nt; $p_{\text{adj}} = 3.66 \times 10^{-9}$), PRPF8 (decrease for TE targets; 2,243nt vs. 2,076nt; $p_{\text{adj}} = 1.03 \times 10^{-8}$), DDX3X (decrease for TE targets; 1,659nt vs 1,376nt; $p_{\text{adj}} = 2.81 \times 10^{-7}$) and G3BP1 (increase for TE targets; 1,985 vs. 2,798nt; $p_{\text{adj}} = 6.11 \times 10^{-8}$).

Some RBPs, including the DEAD-box helicases eIF4A (as part of eIF4F (Svitkin *et al.*, 2001)) and DDX3X (Guenther *et al.*, 2018; Soto-Rifo *et al.*, 2012; Calviello

et al., 2020), regulate translation initiation by interacting with, and subsequently disentangling, highly structured RNA sequences. For instance, DDX3X binds 5' UTRs and the small ribosomal unit to facilitate the translation of a subset of mRNAs with long and structured leader sequences (Calviello *et al.*, 2020). In order to define if additional RBPs may be required for, or involved in, translation initiation at targets with highly structured 5' UTRs, we looked into the 5' UTR minimum free energy (MFE, length normalized) of TE and mRNA target genes of all dual-function RBPs. We observed that, between the positively and negatively correlating target translational efficiencies of 17 out of 21 dual-function RBPs, 5' UTR sequences differed in structural composition (**Figure 4A**), while we observed poor to almost no differences for the significantly correlating mRNA targets of the same RBPs. Strikingly, three RBPs exhibited by far the strongest MFE differences between positively and negatively correlating targets: next to DDX3X ($p_{\text{adj}} = 9.47 \times 10^{-47}$), those were the core spliceosome factors PRPF8 ($p_{\text{adj}} = 2.70 \times 10^{-29}$) and EFTUD2 ($p_{\text{adj}} = 1.69 \times 10^{-30}$) (**Figure 4A** and **4B**). The targets shared between these RBPs displayed similar directions of correlation with the three RBPs (**Figure 4C**) and encode for proteins involved in mRNA stabilization (GO:0048255, $p_{\text{adj}} = 3.09 \times 10^{-4}$).

DISCUSSION

Increasing evidence suggests that RBPs can act as multifunctional gene expression regulators (Backlund *et al.*, 2020; Calviello *et al.*, 2020). Here, we built an in-silico method for the large-scale analysis of RBP-driven regulation using correlation as a proxy for mRNA abundance and translational efficiency (TE) of target genes in the human heart. Our approach underscores the functional importance of RBP expression fluctuations in the control of gene expression, a mechanistic feature recently highlighted by others *in vitro* (Chothani *et al.*, 2019; Luo *et al.*, 2020; Sharma *et al.*, 2021). We exploited the quantitative effect of RBPs on known target genes to implicate 74 RBPs in the regulation of mRNA abundance and translation.

We discovered 27 RBPs with previously unknown roles in translation, some of which have well-characterized functions in other biological processes, including mRNA splicing. Previous work revealed a handful of splicing factors that can mediate post-splicing activities such as mRNA translation (Chen *et al.*, 2019; Maslon *et al.*, 2014; Kim *et al.*, 2014), although the high fraction of splicing factors that we find to influence translation suggests previously unanticipated roles for many more splicing regulators in this process.

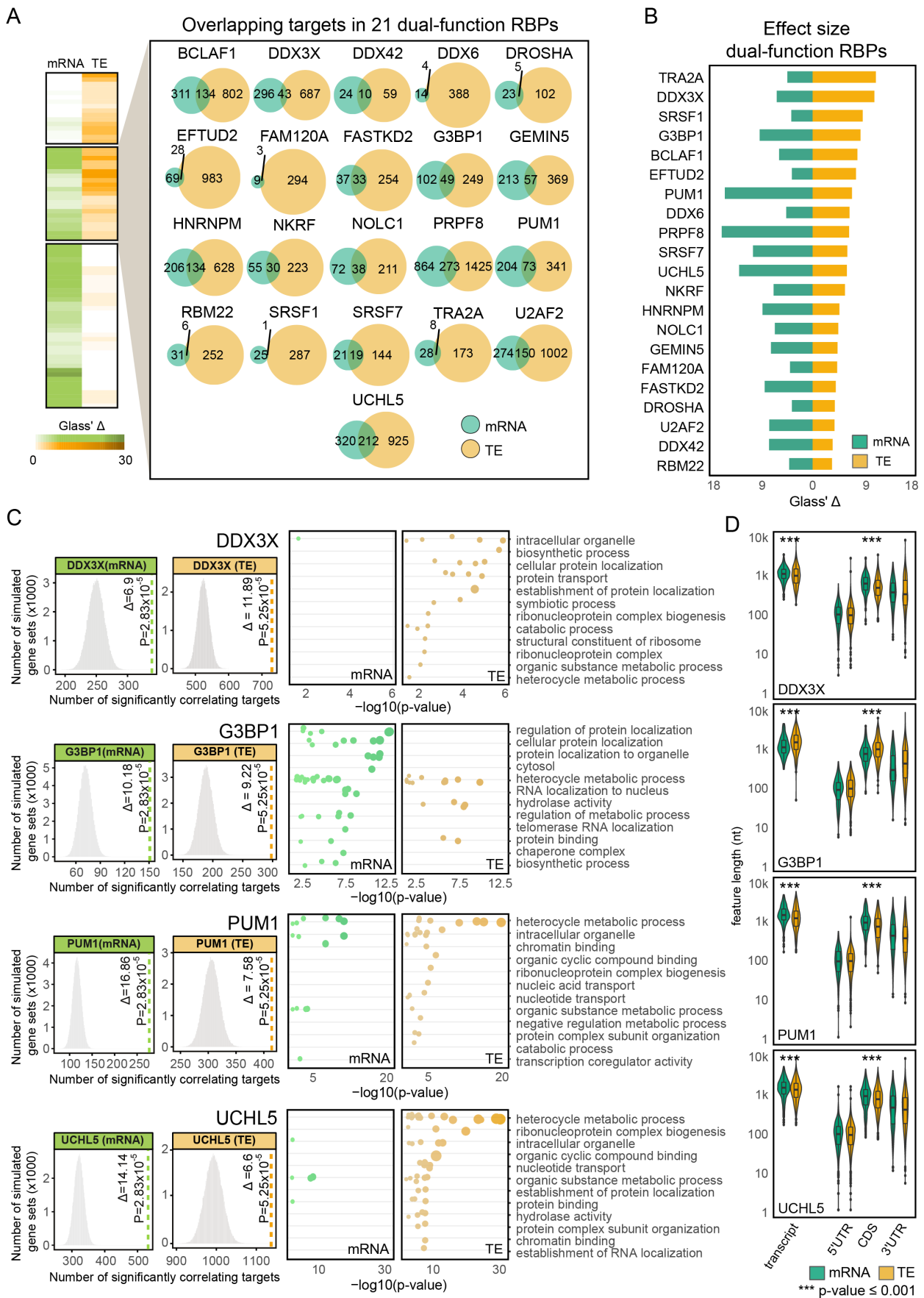


Figure 3. Dual-function RBPs regulate translation of distinct sets of target genes. (A) Heatmap with Glass' Δ scores quantifying the effect size of the witness effects for mRNA and TE correlations. Both effect sizes are significant for a highlighted set of 21 dual-function RBPs. For this set of RBPs, individual Venn Diagrams representing the overlap in the total number of mRNA and TE targets are displayed. **(B)** Bar plot quantifying the magnitude of mRNA and TE effect size (Glass' Δ scores) for dual-function RBPs. RBP effect sizes are largely independent of the mode of regulation. **(C)** Selected histograms and dot plots illustrating the significance of RBP-target correlations and the enrichment of GO terms for the targets bound by 4 dual-function RBPs: DDX3X, G3BP1, PUM1, and UCHL5. For each RBP, the

12 most significant parental GO terms are displayed. mRNA and TE targets exhibit different enrichment of significant GO terms. (D) Box plots with transcript, 5' UTR, CDS, and 3' UTR sequence lengths in nucleotides for mRNA and TE targets corresponding to the four selected dual-function RBPs in (C). A total of 9 dual-function RBPs bind targets with significantly different CDS lengths. See also Figure S3.

A prominent example is the muscle-specific and cardiac disease-relevant splicing regulator RBM20. We for the first time demonstrate that RBM20 expression correlates positively with the TE of many sarcomere genes, suggesting that the nuclear splicing control can impact cytoplasmic protein synthesis. Further functional studies could determine whether isoform-specific characteristics intrinsic to an mRNA, such as the 'swiftness' of nuclear export (Kim & Myong, 2016), secondary transcript structure (Lim et al., 2018; Wang et al., 2020), or codon usage (Drummond & Wilke, 2008; Qian et al., 2012), contribute to the observed differences in TE. Inferring isoform-specific changes in translation rates as a consequence of altered RBP levels is likely complex: highly structured 5' UTRs can decrease the efficiency of translation initiation at the cost of an overall lower translational output (Leppek et al., 2018; Pelletier & Sonenberg, 1985), whereas increased RNA structures may also enhance transcript stability and hence mRNA half-life, in turn yielding higher protein output over time (Mauger et al., 2019).

Besides the discovery of potential novel functions for a subset of RBPs, we provide evidence that 21 RBPs can modulate both target mRNA abundance and TE - a class of RBPs that we classify as "dual-function RBPs". Interestingly, dual-function RBPs appear to be involved in the regulation of mRNA abundance and TE of distinct groups of target genes. These target genes can be concordantly or discordantly regulated on either layer of gene expression control. Although the precise RBP mechanisms behind this dual functionality will require more follow-up, we discovered that the specific affinity of several RBPs to structural properties of mRNAs, such as protein-coding sequence length, UTR length or RNA secondary structure, contribute separately to the observed independent effects on mRNA abundance or translation. In support of our findings, a recent study (Sharma et al., 2021) has inspected the connection between the binding kinetics of the RBP DAZL and their effect on mRNA abundance and translation of specific sets of target genes, identifying several 3' UTR features - UTR length, presence of binding clusters, distance to the polyadenylation site - that are linked to the trait-specific regulation of different groups of targets. In addition, the usage of different ribosome binding domains, the recognition of alternative RBP motifs and the presence of binding sites located in different gene regions (i.e., UTRs, CDS, or introns) can be also indicative of RBP multi-functionality (Ray et al., 2013). Nevertheless, we found these mRNA characteristics to remain largely unchanged for the targets of dual-function RBPs identified in this study.

For a subgroup of dual-function RBPs, we noticed that the targets regulated on the transcriptional or translational level represent functionally different gene classes. This biological diversity seems to match the condition-specific regulatory complexity that needs to be achieved by a single RBP. For instance, this appears to be the case for G3BP1 - a known multi-functional RBP that can selectively compartmentalize specific sets of mRNAs to stress granules, in order to reprogram mRNA translation under certain stress conditions (Matsuki et al., 2013; Ying & Khapersky, 2021; Sahoo

et al., 2018). Additionally, G3BP1 plays an important role in DNA/RNA unwinding (Costa et al., 1999) and binds to specific RNA stem-loop structures to trigger mRNA degradation (Fischer et al., 2020), which is essential for maternal mRNA clearance (Laver et al., 2020). Another example is DDX3X, a DEAD box helicase which can respond to stressors (e.g., viral infections (Yedavalli et al., 2004)) by switching subcellular compartments. DDX3X is involved in multiple processes required for RNA metabolism (Mo et al., 2021; Soto-Rifo et al., 2012), for which it uses its capacity to unwind complex and structured 5' UTRs to promote translation initiation at selected subsets of mRNAs (Soto-Rifo et al., 2012; Guenther et al., 2018; Calviello et al., 2020; Shen & Pelletier, 2020). However, there is ongoing debate as to the precise roles of DDX3X and the mechanisms through which it regulates RNA metabolism (Shen & Pelletier, 2020), as it can act both as a repressor or activator of translation (Hilliker et al., 2011).

Our work points to an intricate relation between the direction of translation regulation and target 5' UTR structure, with the TE rates of certain targets being positively or negatively influenced by RBP binding depending on the complexity of target 5' UTR sequences. Unexpectedly, our results show that increased levels of DDX3X correlate with a lower TE for targets with highly structured 5' UTRs. This contradicts recent *in vitro* reports where DDX3X knockdown in human cells (Calviello et al., 2020) resulted in translational repression of mRNAs with structured 5' UTRs. Next to DDX3X, the strongest impact of the 5' UTR on translational output is observed for EFTUD2 and PRPF8, which display patterns of regulation highly similar to DDX3X, suggesting an analogous mode of action in the control of target translation rates. Surprisingly, EFTUD2 and PRPF8 are splicing factors which are part of the central component of the U5 snRNP spliceosome (Malinová et al., 2017) and had not been implicated in translation before. However, the conserved GTPase EFTUD2 has sequence similarity to the translation elongation factor EF-2 (Fabrizio et al., 1997), possibly explaining its capacity to influence translation. Both ancient paralogs may have evolved and diversified to complement each other.

Whereas dual functionality of extensively studied and characterized RBPs such as DDX3X and G3BP1 had (to a certain extent) been described previously, for a selection of other RBPs our results provide initial observations of dual functionality. For instance, UCHL5 (also known as UCH37) is a protease with RNA binding capacity that may be part of the INO80 chromatin remodeling complex (Yao et al., 2008), though its role within RNA metabolism is yet unknown. We establish a quantitative relationship between UCHL5 expression and variability in mRNA abundance of genes involved in chromatin organization, as well as with changes in TE of genes involved in RNA splicing. Although UCHL5 shares target genes with core splicing factors (U2AF2, EFTUD2 and PRPF8), its effect on the TE of targets shared with these three splicing factors is completely opposite, suggesting contrasting regulatory behavior, and possibly competition.

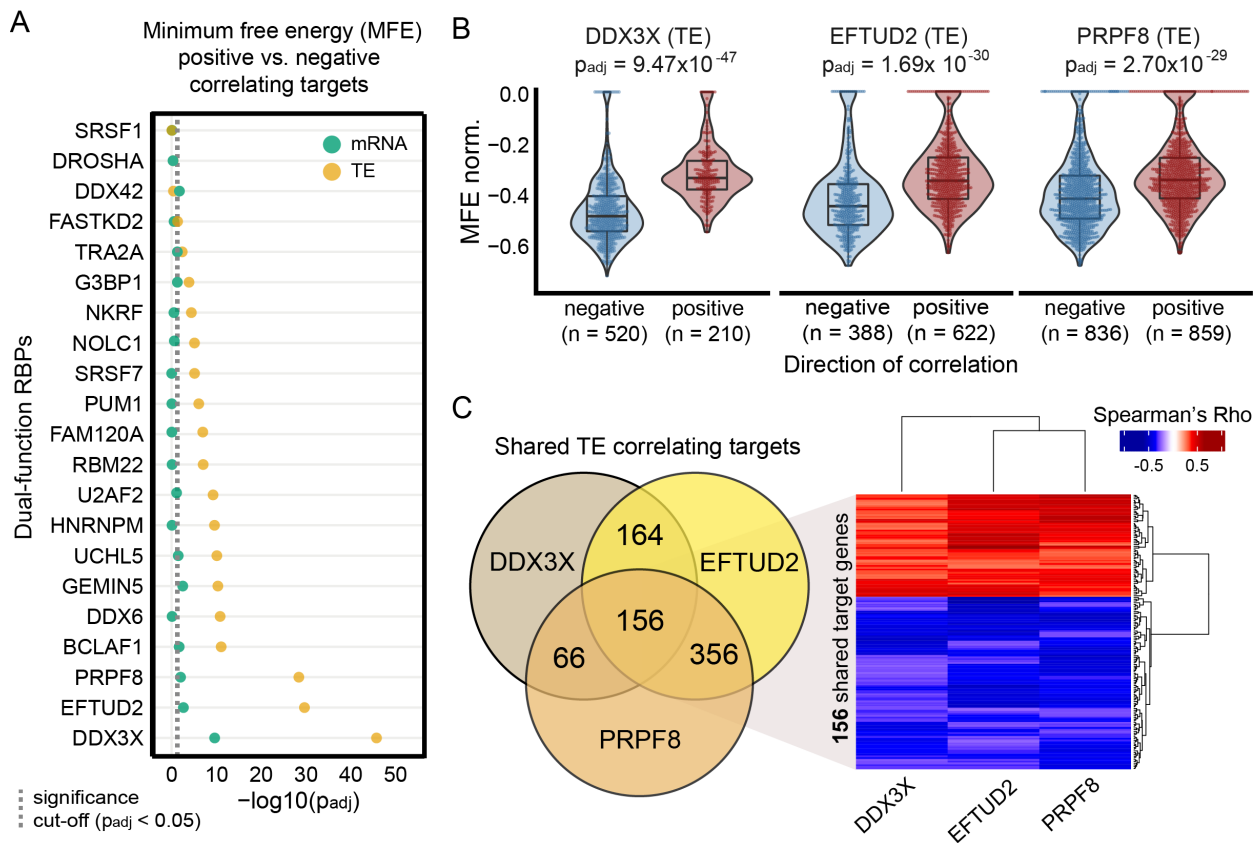


Figure 4. Differential affinity of dual-function RBPs for 5' UTR structures often drives opposite quantitative TE effects. (A) Dot plot displaying the significance of the differences in 5' UTR minimum free energy (MFE, normalized by length) between target genes that correlate positively or negatively with each dual-function RBP. Significance values are calculated separately for mRNA (green) and TE (brown) targets. Adjusted p-values are shown on $-\log_{10}$ scale and calculated using the Wilcoxon Rank Sum test and only 5' UTR sequences with a minimum length of 20 nucleotides were evaluated. A dashed vertical line indicates the minimum adjusted p-value to consider the differences in MFE as significant ($p_{adj} < 0.05$). **(B)** Box and violin plots with length normalized MFE scores for positively and negatively correlated TE targets corresponding to the three selected dual-function RBPs with the highest significance in Figure 4A (DDX3X, EFTUD2, PRPF8). **(C)** Three-way Venn Diagram representing the overlap in the number of TE targets for the three selected RBPs. The heatmap represents TE correlations of 156 shared target genes for the three selected dual-function RBPs.

Very little is known about the molecular processes that control RBP multi-functionality, although some possible mechanisms have been recently investigated, including the formation of heterogeneous RBP complexes (Copsey et al., 2017; Damianov et al., 2016), switches from monomers to multimers in a concentration-dependent manner (Kim & Myong, 2016), and changes in subcellular localization (Chen et al., 2019; Burgess et al., 2011). In our current study, the potential mechanisms behind the observed dual functionality could not be explained in a uniform way: there appears to be no 'one size fits all' scenario. It is very probable that RBP multi-functionality is achieved by specific combinations of individual RBP and target features, whose precise dissection requires experimental follow-up into each individual dual-function RBP. An RBP may bind distinct sets of RNA within the nucleus, though, for a subset of targets, the consequences of binding may only become apparent at a later stage of gene expression (e.g., a change in transcript isoform production that is accompanied by a downstream effect on TE). Alternatively, dual-function RBPs may physically take part in multiple stages of gene expression by adapting

subcellular localizations. For instance, HNRNPM (one of the core splicing ribonucleoproteins that we found to influence both target gene mRNA abundance and TE) localizes to nucleus (Harvey et al., 2018) but can be exported to the cytosol to induce cap-independent translation upon hypoxia (Chen et al., 2019). Another example, DDX3X, shuttles between nucleus and cytosol (Yedavalli et al., 2004). It remains to be established if RBPs with shared targets bind these targets simultaneously, or in a sequential order. RBP abundance may also respond to target availability and not vice versa, possibly explaining why we find many splicing regulators to rank highly within the RBP hierarchy.

In conclusion, our results illustrate unanticipated complexity in RBP-RNA interactions at multiple consecutive levels of gene expression. Understanding how RBPs cooperate, communicate, interact and compete across subcellular compartments and in response to changing conditions will be essential to fully comprehend the quantitative nature of the regulatory principles that underlie mRNA metabolism.

DATA AVAILABILITY

All code used for the analyses in this paper is available upon request.

ACKNOWLEDGEMENTS

We would like to thank Prof. Dr. Markus Landthaler for his helpful feedback and discussions. N.H. is recipient of an ERC advanced grant under the European Union's Horizon 2020 research and innovation programme (grant agreement n° AdG788970). N.H. is supported by a grant from the Leducq Foundation (11 CVD-01). N.H. was supported by the "Bundesministerium für Bildung und Forschung" under grant CaRNAtion.

AUTHOR CONTRIBUTIONS

Conceptualization, V.S-L., J. R-O., N.H. and S.v.H.; Methodology, V.S-L., J. R-O. and S.v.H.; Software, V.S-L., J. R-O.; Formal Analysis, V.S-L.; Investigation, V.S-L., J. R-O. and S.v.H.; Writing – Original Draft, V.S-L., J. R-O. and S.v.H.; Writing - Review and Editing, all authors; Visualization, V.S-L., J. R-O. and S.v.H.; Funding Acquisition, N.H.; Supervision, S.v.H. and N.H.

Declaration of Interests

The authors declare no competing interest

REFERENCES

- Ainaoui N., Hantelys F., Renaud-Gabardos E., Bunel M., Lopez F., Pujol F., Planes R., Bahraoui E., Pichereaux C., Burlet-Schiltz O., et al. (2015). Promoter-Dependent Translation Controlled by p54nrb and hnRNPM during Myoblast Differentiation. *PLoS one* 10.(9). Ed. by Y. K. Kim, e0136466.
- Anders S., Pyl P. T. & Huber W. (2015). HTSeq—a Python framework to work with high-throughput sequencing data. *Bioinformatics* (Oxford, England) 31.(2), 166–9.
- Backlund M., Stein F., Rettel M., Schwarzl T., Perez-Perri J. I., Brosig A., Zhou Y., Neu-Yilik G., Hentze M. W. & Kulozik A. E. (2020). Plasticity of nuclear and cytoplasmic stress responses of RNA-binding proteins. *Nucleic acids research* 48.(9), 4725–4740.
- Beckmann B. M., Castello A. & Medenbach J. (2016). The expanding universe of ribonucleoproteins: of novel RNA-binding proteins and unconventional interactions. *Pflugers Archiv : European journal of physiology* 468.(6), 1029–40.
- Benjamini Y. & Hochberg Y. (1995). Controlling the False Discovery Rate: A Practical and Powerful Approach to Multiple Testing. *Journal of the Royal Statistical Society: Series B (Methodological)* 57.(1), 289–300.
- Benoit Bouvrette L. P., Bovaird S., Blanchette M. & Lécuyer E. (2020). oRNAment: a database of putative RNA binding protein target sites in the transcriptomes of model species. *Nucleic acids research* 48.(D1), D166–D173.
- Buchan J. R. (2014). mRNP granules. Assembly, function, and connections with disease. *RNA biology* 11.(8), 1019–30.
- Burgess H. M., Richardson W. A., Anderson R. C., Salaun C., Graham S. V. & Gray N. K. (2011). Nuclear relocalisation of cytoplasmic poly(A)-binding proteins PABP1 and PABP4 in response to UV irradiation reveals mRNA-dependent export of metazoan PABPs. *Journal of cell science* 124.(Pt 19), 3344–55.
- Calviello L., Venkataramanan S., Rogowski K. J., Wyler E., Wilkins K., Tejura M., Thai B., Krol J., Filipowicz W., Landthaler M., et al. (2020). DDX3 depletion represses translation of mRNAs with complex 5' UTRs. *bioRxiv*, 589218.
- Castello A., Fischer B., Frese C. K., Horos R., Alleaume A.-M., Foehr S., Curk T., Krijgsvelde J. & Hentze M. W. (2016). Comprehensive Identification of RNA-Binding Domains in Human Cells. *Molecular cell* 63.(4), 696–710.
- Caudron-Herger M., Rusin S. F., Adamo M. E., Seiler J., Schmid V. K., Barreau E., Kettenbach A. N. & Diederichs S. (2019). R-DeeP: Proteome-wide and Quantitative Identification of RNA-Dependent Proteins by Density Gradient Ultracentrifugation. *Molecular cell* 75.(1), 184–199.e10.
- Chen T.-M., Lai M.-C., Li Y.-H., Chan Y.-L., Wu C.-H., Wang Y.-M., Chien C.-W., Huang S.-Y., Sun H. S. & Tsai S.-J. (2019). hnRNPM induces translation switch under hypoxia to promote colon cancer development. *EBioMedicine* 41, 299–309.
- Chothani S., Schäfer S., Adami E., Viswanathan S., Widjaja A. A., Langley S. R., Tan J., Wang M., Quaipe N. M., Jian Pua C., et al. (2019). Widespread Translational Control of Fibrosis in the Human Heart by RNA-Binding Proteins. *Circulation* 140.(11), 937–951.
- Cirillo L., Cieren A., Barbieri S., Khong A., Schwager F., Parker R. & Gotta M. (2020). UBAP2L Forms Distinct Cores that Act in Nucleating Stress Granules Upstream of G3BP1. *Current biology : CB* 30.(4), 698–707.e6.
- Copsey A. C., Cooper S., Parker R., Lineham E., Lapworth C., Jallad D., Sweet S. & Morley S. J. (2017). The helicase, DDX3X, interacts with poly(A)-binding protein 1 (PABP1) and caprin-1 at the leading edge of migrating fibroblasts and is required for efficient cell spreading. *The Biochemical journal* 474.(18), 3109–3120.
- Costa M., Ochem A., Staub A. & Falaschi A. (1999). Human DNA helicase VIII: a DNA and RNA helicase corresponding to the G3BP protein, an element of the ras transduction pathway. *Nucleic acids research* 27.(3), 817–21.
- Damianov A., Ying Y., Lin C.-H., Lee J.-A., Tran D., Vashisht A. A., Bahrami-Samani E., Xing Y., Martin K. C., Wohlschlegel J. A., et al. (2016). Rbfox Proteins Regulate Splicing as Part of a Large Multiprotein Complex LASR. *Cell* 165.(3), 606–19.
- Dassi E. (2017). Handshakes and Fights: The Regulatory Interplay of RNA-Binding Proteins. *Frontiers in molecular biosciences* 4, 67.
- Davis C. A., Hitz B. C., Sloan C. A., Chan E. T., Davidson J. M., Gabdank I., Hilton J. A., Jain K., Baymuradov U. K., Narayanan A. K., et al. (2018). The Encyclopedia of DNA elements (ENCODE): data portal update. *Nucleic acids research* 46.(D1), D794–D801.
- Díaz-Muñoz M. D. & Turner M. (2018). Uncovering the Role of RNA-Binding Proteins in Gene Expression in the Immune System. *Frontiers in immunology* 9.(MAY), 1094.
- Dobin A., Davis C. A., Schlesinger F., Drenkow J., Zaleski C., Jha S., Batut P., Chaisson M. & Gingeras T. R. (2013). STAR: ultrafast universal RNA-seq aligner. *Bioinformatics* (Oxford, England) 29.(1), 15–21.
- Dong J., Aitken C. E., Thakur A., Shin B. S., Lorsch J. R. & Hinnebusch A. G. (2017). Rps3/uS3 promotes mRNA binding at the 40S ribosome entry channel and stabilizes preinitiation complexes at start codons. *Proceedings of the National Academy of Sciences of the United States of America*.
- Drummond D. A. & Wilke C. O. (2008). Mistranslation-induced protein misfolding as a dominant constraint on coding-sequence evolution. *Cell* 134.(2), 341–52.
- Fabrizio P., Laggerbauer B., Lauber J., Lane W. S. & Lührmann R. (1997). An evolutionarily conserved U5 snRNP-specific protein is a GTP-binding factor closely related to the ribosomal translocase EF-2. *The EMBO journal* 16.(13), 4092–106.
- Fischer J. W., Busa V. F., Shao Y. & Leung A. K. L. (2020). Structure-Mediated RNA Decay by UPF1 and G3BP1. *Molecular cell* 78.(1), 70–84.e6.
- Freeman P. R., Hedges L. V. & Olkin I. (1986). *Statistical Methods for Meta-Analysis*. *Biometrics* 42.(2), 454.
- Gerstberger S., Hafner M. & Tuschl T. (2014). A census of human RNA-binding proteins. *Nature reviews. Genetics* 15.(12), 829–45.
- Gilbertson S., Federspiel J. D., Hartenian E., Cristea I. M. & Glaunsinger B. (2018). Changes in mRNA abundance drive shuttling of RNA binding proteins, linking cytoplasmic RNA degradation to transcription. *eLife* 7.
- Gray N. K., Hrabáková L., Scanlon J. P. & Smith R. W. P. (2015). Poly(A)-binding proteins and mRNA localization: who rules the roost? *Biochemical Society transactions* 43.(6), 1277–1284.
- GTEX Consortium (2013). The Genotype-Tissue Expression (GTEx) project. *Nature genetics* 45.(6), 580–5.
- Guenther U.-P., Weinberg D. E., Zubradt M. M., Tedeschi F. A., Stawicki B. N., Zagore L. L., Brar G. A., Licatalosi D. D., Bartel D. P., Weissman J. S., et al. (2018). The helicase Ded1p controls use of near-cognate translation initiation codons in 5' UTRs. *Nature* 559.(7712), 130–134.
- Guo W., Schafer S., Greaser M. L., Radke M. H., Liss M., Govindarajan T., Maatz H., Schulz H., Li S., Parrish A. M., et al. (2012). RBM20, a gene for hereditary cardiomyopathy, regulates titin splicing. *Nature medicine* 18.(5), 766–73.
- Gysi D. M., Voigt A., Fragoso T. d. M., Almaas E. & Nowick K. (2018). wTO: an R package for computing weighted topological overlap and a consensus network with integrated visualization tool. *BMC bioinformatics* 19.(1), 392.
- Hannon G. (2010). FASTX-Toolkit.
- Harvey R. F., Smith T. S., Mulrone T., Queiroz R. M. L., Pizzinga M., Dezi V., Villeneuve E., Ramakrishna M., Lilley K. S. & Willis A. E. (2018). Trans-acting translational regulatory RNA binding proteins. *Wiley interdisciplinary reviews. RNA* 9.(3), e1465.
- Hilliker A., Gao Z., Jankowsky E. & Parker R. (2011). The DEAD-box protein Ded1 modulates translation by the formation and resolution of an eIF4F-mRNA complex. *Molecular cell* 43.(6), 962–72.
- Hinnebusch A. G. (2014). The scanning mechanism of eukaryotic translation initiation. *Annual review of biochemistry* 83, 779–812.
- Kim J., Park R. Y., Chen J.-K., Kim J., Jeong S. & Ohn T. (2014). Splicing factor SRSF3 represses the translation of programmed cell

- death 4 mRNA by associating with the 5'-UTR region. *Cell death and differentiation* 21.(3), 481–90.
- Kim Y. & Myong S. (2016). RNA Remodeling Activity of DEAD Box Proteins Tuned by Protein Concentration, RNA Length, and ATP. *Molecular cell* 63.(5), 865–76.
- Kong X., Chen Y.-Y., Lin J., Flowers E., Van Nostrand E., Blue S. M., Chau J., Ma C. I.-H., Mohr I., Thai R., et al. (2019). The cohesin loader NIPBL interacts with pre-ribosomal RNA and treacle to regulate ribosomal RNA synthesis. *bioRxiv*.
- Laver J. D., Ly J., Winn A. K., Karaiskakis A., Lin S., Nie K., Benic G., Jaberi-Lashkari N., Cao W. X., Khademi A., et al. (2020). The RNA-Binding Protein Rasputin/G3BP Enhances the Stability and Translation of Its Target mRNAs. *Cell reports* 30.(10), 3353–3367.e7.
- Leppek K., Das R. & Barna M. (2018). Functional 5' UTR mRNA structures in eukaryotic translation regulation and how to find them. *Nature reviews. Molecular cell biology* 19.(3), 158–174.
- Li Q., Brown J. B., Huang H. & Bickel P. J. (2011). Measuring reproducibility of high-throughput experiments. *The Annals of Applied Statistics* 5.(3), 1752–1779.
- Lieberman N., Marash L. & Kimchi A. (2009). The translation initiation factor DAP5 is a regulator of cell survival during mitosis. *Cell cycle (Georgetown, Tex.)* 8.(2), 204–9.
- Lim C. S., T Wardell S. J., Kleffmann T. & Brown C. M. (2018). The exon-intron gene structure upstream of the initiation codon predicts translation efficiency. *Nucleic acids research* 46.(9), 4575–4591.
- Love M. I., Huber W. & Anders S. (2014). Moderated estimation of fold change and dispersion for RNA-seq data with DESeq2. *Genome biology* 15.(12), 550.
- Luo E.-C., Nathanson J. L., Tan F. E., Schwartz J. L., Schmok J. C., Shankar A., Markmiller S., Yee B. A., Sathe S., Pratt G. A., et al. (2020). Large-scale tethered function assays identify factors that regulate mRNA stability and translation. *Nature structural & molecular biology* 27.(10), 989–1000.
- Maatz H., Jens M., Liss M., Schafer S., Heinig M., Kirchner M., Adami E., Rintisch C., Dauksaite V., Radke M. H., et al. (2014). RNA-binding protein RBM20 represses splicing to orchestrate cardiac pre-mRNA processing. *The Journal of clinical investigation* 124.(8), 3419–30.
- Malinová A., Cvačková Z., Matějů D., Hořejší Z., Abéza C., Vandermoere F., Bertrand E., Staněk D. & Verheggen C. (2017). Assembly of the U5 snRNP component PRPF8 is controlled by the HSP90/R2TP chaperones. *The Journal of cell biology* 216.(6), 1579–1596.
- Mallam A. L., Sae-Lee W., Schaub J. M., Tu F., Battenhouse A., Jang Y. J., Kim J., Wallingford J. B., Finkelstein I. J., Marcotte E. M., et al. (2019). Systematic Discovery of Endogenous Human Ribonucleoprotein Complexes. *Cell reports* 29.(5), 1351–1368.e5.
- Maslon M. M., Heras S. R., Bellora N., Eyraş E. & Cáceres J. F. (2014). The translational landscape of the splicing factor SRSF1 and its role in mitosis. *eLife* 3.
- Matsuki H., Takahashi M., Higuchi M., Makokha G. N., Oie M. & Fujii M. (2013). Both G3BP1 and G3BP2 contribute to stress granule formation. *Genes to cells : devoted to molecular & cellular mechanisms* 18.(2), 135–46.
- Mauger D. M., Cabral B. J., Presnyak V., Su S. V., Reid D. W., Goodman B., Link K., Khatwani N., Reynders J., Moore M. J., et al. (2019). mRNA structure regulates protein expression through changes in functional half-life. *Proceedings of the National Academy of Sciences of the United States of America* 116.(48), 24075–24083.
- Mo J., Liang H., Su C., Li P., Chen J. & Zhang B. (2021). DDX3X: structure, physiologic functions and cancer. *Molecular cancer* 20.(1), 38.
- Müller-McNicoll M. & Neugebauer K. M. (2013). How cells get the message: dynamic assembly and function of mRNA-protein complexes. *Nature reviews. Genetics* 14.(4), 275–87.
- Nott A., Le Hir H. & Moore M. J. (2004). Splicing enhances translation in mammalian cells: an additional function of the exon junction complex. *Genes & development* 18.(2), 210–22.
- Nowick K., Gernat T., Almaas E. & Stubbs L. (2009). Differences in human and chimpanzee gene expression patterns define an evolving network of transcription factors in brain. *Proceedings of the National Academy of Sciences of the United States of America* 106.(52), 22358–63.
- Pelletier J. & Sonenberg N. (1985). Insertion mutagenesis to increase secondary structure within the 5' noncoding region of a eukaryotic mRNA reduces translational efficiency. *Cell* 40.(3), 515–26.
- Qian W., Yang J.-R., Pearson N. M., Maclean C. & Zhang J. (2012). Balanced codon usage optimizes eukaryotic translational efficiency. *PLoS genetics* 8.(3), e1002603.
- Quinlan A. R. & Hall I. M. (2010). BEDTools: a flexible suite of utilities for comparing genomic features. *eng. Bioinformatics (Oxford, England)* 26.(6), 841–2.
- R Core Team (2020) (2020). R: A language and environment for statistical computing.
- Raudvere U., Kolberg L., Kuzmin I., Arak T., Adler P., Peterson H. & Vilo J. (2019). g:Profiler: a web server for functional enrichment analysis and conversions of gene lists (2019 update). *Nucleic acids research* 47.(W1), W191–W198.
- Ray D., Kazan H., Cook K. B., Weirauch M. T., Najafabadi H. S., Li X., Gueroussov S., Albu M., Zheng H., Yang A., et al. (2013). A compendium of RNA-binding motifs for decoding gene regulation. *Nature* 499.(7457), 172–7.
- Sahoo P. K., Lee S. J., Jaiswal P. B., Alber S., Kar A. N., Miller-Randolph S., Taylor E. E., Smith T., Singh B., Ho T. S.-Y., et al. (2018). Axonal G3BP1 stress granule protein limits axonal mRNA translation and nerve regeneration. *Nature communications* 9.(1), 3358.
- Schafer S., Miao K., Benson C. C., Heinig M., Cook S. A. & Hubner N. (2015a). Alternative Splicing Signatures in RNA-seq Data: Percent Spliced in (PSI). *Current protocols in human genetics* 87, 11.16.1–11.16.14.
- Schafer S., Adami E., Heinig M., Rodrigues K. E. C., Kreuchwig F., Silhavy J., Heesch S. van, Simaite D., Rajewsky N., Cuppen E., et al. (2015b). Translational regulation shapes the molecular landscape of complex disease phenotypes. *Nature communications* 6, 7200.
- Sharma D., Zagore L. L., Brister M. M., Ye X., Crespo-Hernández C. E., Licatalosi D. D. & Jankowsky E. (2021). The kinetic landscape of an RNA-binding protein in cells. *Nature* 591.(7848), 152–156.
- Shen L. & Pelletier J. (2020). General and Target-Specific DExD/H RNA Helicases in Eukaryotic Translation Initiation. *International journal of molecular sciences* 21.(12).
- Shi Z., Fujii K., Kovary K. M., Genuth N. R., Röst H. L., Teruel M. N. & Barna M. (2017). Heterogeneous Ribosomes Preferentially Translate Distinct Subpools of mRNAs Genome-wide. *Molecular cell* 67.(1), 71–83.e7.
- Simsek D., Tiu G. C., Flynn R. A., Byeon G. W., Leppek K., Xu A. F., Chang H. Y. & Barna M. (2017). The Mammalian Ribo-interactome Reveals Ribosome Functional Diversity and Heterogeneity. *Cell* 169.(6), 1051–1065.e18.
- Soto-Rifo R., Rubilar P. S., Limousin T., Breyne S. de, Décimo D. & Ohlmann T. (2012). DEAD-box protein DDX3 associates with eIF4F to promote translation of selected mRNAs. *The EMBO journal* 31.(18), 3745–56.
- Sutherland L. C., Wang K. & Robinson A. G. (2010). RBM5 as a putative tumor suppressor gene for lung cancer.
- Svitkin Y. V., Pause A., Haghhighat A., Pyronnet S., Witherell G., Belsham G. J. & Sonenberg N. (2001). The requirement for eukaryotic initiation factor 4A (eIF4A) in translation is in direct proportion to the degree of mRNA 5' secondary structure. *RNA (New York, N.Y.)* 7.(3), 382–94.
- Szklarczyk D., Gable A. L., Lyon D., Junge A., Wyder S., Huerta-Cepas J., Simonovic M., Doncheva N. T., Morris J. H.,

- Bork P., et al. (2019). STRING v11: protein-protein association networks with increased coverage, supporting functional discovery in genome-wide experimental datasets. *Nucleic acids research* 47.(D1), D607–D613.
- Trendel J., Schwarzl T., Horos R., Prakash A., Bateman A., Hentze M. W. & Krijgsveld J. (2019). The Human RNA-Binding Proteome and Its Dynamics during Translational Arrest. *Cell* 176.(1-2), 391–403.e19.
- Van Heesch S., Witte F., Schneider-Lunitz V., Schulz J. F., Adami E., Faber A. B., Kirchner M., Maatz H., Blachut S., Sandmann C.-L., et al. (2019). The Translational Landscape of the Human Heart. *Cell* 178.(1), 242–260.e29.
- Van Nostrand E. L., Freese P., Pratt G. A., Wang X., Wei X., Xiao R., Blue S. M., Chen J.-Y., Cody N. A. L., Dominguez D., et al. (2020). A large-scale binding and functional map of human RNA-binding proteins. *Nature* 583.(7818), 711–719.
- Wang S. E., Brooks A. E. S., Poole A. M. & Simoes-Barbosa A. (2020). Determinants of translation efficiency in the evolutionarily-divergent protist *Trichomonas vaginalis*. *BMC molecular and cell biology* 21.(1), 54.
- Weber R, Kleemann L, Hirschberg I, Chung M, Valkov E I. C. (2021). DAP5 enables translation re-initiation on structured messenger RNAs. *bioRxiv*.
- Yang W., Ru Y., Ren J., Bai J., Wei J., Fu S., Liu X., Li D. & Zheng H. (2019). G3BP1 inhibits RNA virus replication by positively regulating RIG-I-mediated cellular antiviral response. *Cell death & disease* 10.(12), 946.
- Yao T., Song L., Jin J., Cai Y., Takahashi H., Swanson S. K., Washburn M. P., Florens L., Conaway R. C., Cohen R. E., et al. (2008). Distinct Modes of Regulation of the Uch37 Deubiquitinating Enzyme in the Proteasome and in the Ino80 Chromatin-Remodeling Complex. *Molecular Cell*.
- Yedavalli V. S.R. K., Neuveut C., Chi Y.-H., Kleiman L. & Jeang K.-T. (2008). Requirement of DDX3 DEAD box RNA helicase for HIV-1 Rev-RRE export function. *Cell* 119.(3), 381–92.
- Ying S. & Khapersky D. A. (2021). UV damage induces G3BP1-dependent stress granule formation that is not driven by mTOR inhibition-mediated translation arrest. *Journal of Cell Science*.
- Yugami M., Okano H., Nakanishi A. & Yano M. (2020). Analysis of the nucleocytoplasmic shuttling RNA-binding protein HNRNPU using optimized HITS-CLIP method. *PloS one* 15.(4), e0231450.
- Zhong Y., Karaletsos T., Drewe P., Sreedharan V. T., Kuo D., Singh K., Wendel H.-G. & Ratsch G. (2017). RiboDiff: detecting changes of mRNA translation efficiency from ribosome footprints. *Bioinformatics (Oxford, England)* 33.(1), 139–141.
- Zhou Z., Dang Y., Zhou M., Li L., Yu C.-H., Fu J., Chen S. & Liu Y. (2016). Codon usage is an important determinant of gene expression levels largely through its effects on transcription. *Proceedings of the National Academy of Sciences of the United States of America* 113.(41), E6117–E6125.

MATERIALS AND METHODS

Ribosome profiling and RNA sequencing data analysis

We re-analyzed ribosome profiling (Ribo-seq) and matched RNA-seq datasets from 80 human hearts that we generated and published previously (EGA accession code: EGAS00001003263) (Van Heesch et al., 2019). In short, Ribo-seq reads were clipped for residual adapters using FASTX toolkit (Hannon, 2010). Reads mapping to the mitochondrial RNA, ribosomal RNA and tRNA sequences were removed from downstream analysis. Full length paired mRNA-seq reads (2×101 nt) were trimmed to 29-mers (average length of Ribo-seq reads) so as to establish a comparable analysis of both Ribo-seq and mRNA-seq datasets and avoid any mapping or quantification bias due to different read length or filtering. Next, Ribo-seq and trimmed mRNA-seq reads were mapped to the human reference genome (GRCh38, Ensembl v87) using STAR v2.5.2b (Dobin et al., 2013) with maximum of 2 mismatches and `-seedSearchStartLmaxOverLread = 0.5`. Quantification of gene expression was performed by counting reads mapping to coding sequence (CDS) regions of annotated protein-coding genes, using HTSeq v0.9.1 (Anders et al., 2015). Gene counts were normalized by estimating the size factors simultaneously on Ribo-seq and RNA-seq datasets using DESeq2 v1.12.4 (Love et al., 2014). This joint normalization is required to compare both measures of gene expression (Zhong et al., 2017). Translational efficiency (TE) was calculated on the Ribo-seq against RNA-seq ratio for each individual gene and sample, as described previously (Van Heesch et al., 2019).

Identification of RBP targets from published eCLIP and HITS-CLIP data

Processed eCLIP data of 150 RBPs were obtained from ENCODE (Davis et al., 2018) for HepG2 ($n = 103$) and K562 ($n = 120$) cell lines. Datasets consisted of BED files containing called eCLIP peaks and BAM files containing reads mapped to the human genome (GRCh38.p10/hg38). The identification of robust eCLIP peaks across replicates and cell lines was performed as suggested by Van Nostrand and colleagues (Van Nostrand et al., 2020). First, we used BEDTools (Quinlan & Hall, 2010) to quantify the coverage of each predicted peak using input (mock) and immunoprecipitation (IP, antibody against RBP) BAM files. Next, for each peak, the relative information content was defined as $p_i \times \log_2(p_i/q_i)$, where p and q are the sums of reads mapping to the peak in IP and negative control respectively. The information content was used to calculate the Irreproducible Discovery Rate (IDR) (Li et al., 2011), a parameter indicating reproducible peaks across biological replicates. A significant and reproducible peak was defined meeting an IDR cut-off < 0.01 , p -value $\leq 10^{-5}$ and fold-enrichment (FC) > 8 . In case two or more peaks overlapped the same genomic region, the most significant one was included in the peak table. Additionally, non-overlapping peaks were pooled into a single table, in order to get a complete set in both cell lines. For the muscle-specific splicing repressor RBM20, which was not part of the ENCODE dataset but included for its importance for cardiac splicing and heart disease (Maatz et al., 2014; Guo et al., 2012), significant RBM20 HITS-CLIP targets were obtained from Maatz et al. (Maatz et al., 2014). Only 143 RBPs with expression in human heart tissue were kept (mean FPKM across samples > 1 ; 142 ENCODE RBPs and RBM20).

Overall, we retrieved an average of 4,300 eCLIP-seq peaks per experiment. Finally, we mapped these peaks to the annotated transcriptome (Ensembl v.87) and, for each RBP experiment, all the genes supported by at least one CLIP-seq peak were defined as putative target genes.

RBP-target correlation and clustering

For RBP-target correlations and clustering we included genes expressed in the human heart (mean FPKM across samples > 1) with at least one Ribo-seq and mRNA-seq read in a minimum of 20 samples ($n = 11,387$). Next, for pairwise complete observations, we calculated Spearman correlations between the expression level of the RBP (as measured by Ribo-seq) and either target gene mRNA-seq counts or translational efficiency. Only target genes that showed a significant ($p_{adj} \leq 0.05$) correlation after correction for multiple testing using the Benjamini-Hochberg approach (Benjamini & Hochberg, 1995) were retained for downstream analyses. The computed RBP-target correlation matrix was used to calculate the Euclidean distance followed by hierarchical clustering, in order to group RBPs with similar consequences on their target genes. Cluster visualization was done using heatmap.3 (<https://github.com/obigriffith/biostar-tutorials/tree/master/Heatmaps>).

Target gene enrichment

To identify RBPs that are putative modulators of target gene mRNA abundance and/or TE, we calculated the frequency with which target genes supported with CLIP-seq data correlated significantly with each RBP. We leveraged the significance of these correlating associations by generating 100,000 equally sized sets of theoretical targets out of all translated genes in the human heart. For each set, we quantified the amount of significantly correlating genes and compared the theoretical distribution against the actual observation applying an empirical test: *Empirical p-value* = $sum(theoretical\ targets > true\ RBP\ targets) / 100,000$. Empirical p-values were corrected for multiple testing (Benjamini-Hochberg method). RBPs that showed a significant ($p_{adj} \leq 0.05$) enrichment of correlating CLIP-derived target genes were considered as putative regulators of mRNA abundance ($n = 58$) and/or TE ($n = 37$). It should be noted that, because of the fixed number of generated random sets, the minimum empirical p-value that can be calculated after correction for multiple testing is 5.25×10^{-5} . Hence, the empirical test cannot quantify the strength of significance for a specific observation. Instead, we calculated Glass' Delta (Δ) (Freeman et al., 1986) as a measure of the effect size, which is defined as the difference between the two target sets divided by the standard deviation of the theoretical group. *Effect size* = $(true\ RBP\ targets - mean(theoretical\ targets)) / sd(theoretical\ targets)$

RBP expression across GTEx tissues

To determine the patterns of expression of each RBP across human tissues, we obtained expression data from the Genotype-Tissue Expression (GTEx) Project (GTEx Consortium, 2013), a database that comprises a large set of samples corresponding to 54 different human tissues. We used these data to determine the number of tissues with detectable (average TPM ≥ 1) or high (average TPM ≥ 10) expression of a given RBP. An RBP was categorized as ubiquitously expressed if expression was detected in more than 30 tissues.

wTO network

A Weighted Topological Overlap (wTO) (Gysi et al., 2018) analysis was performed to generate a RBP-RBP network. For this target TE and RBP expression level matrix was randomly resampled 400 times followed by calculation of Spearman's correlation and a weight score, denoted as wTO. An RBP-RBP weight with $p_{\text{adj}} \leq 0.05$ was considered as stable and retained for downstream analysis. All the remaining parameters were set to default.

Replication of target regulation using a public fibroblast cohort

We retrieved raw RNA-seq and Ribo-seq data from a cohort of 20 primary cardiac fibroblast cultures stimulated with TGF-beta (Chothani et al., 2019) and used it as a replication cohort. Raw data are available via the gene expression omnibus (GEO submission: GSE131112, GSE123018, GSE131111) repository. Read pre-processing, mapping, gene quantification and correlation analysis were done following the same procedures described above for the heart datasets (see 'Read mapping and gene quantification' and 'RBP-target correlation and clustering' subsections). To prove that the regulatory effect of RBPs in target translational regulation can be replicated in an independent dataset, we quantified the fraction of RBP-target correlations with similar direction of regulation in both fibroblast and human heart cohorts. Statistical significance of the observed replications was evaluated by running 10,000 permutations of the correlation coefficients in fibroblasts and comparing the fraction of shared directionality between both cohorts in observed and randomized sets.

Analysis of differential exon splicing

To evaluate whether RBM20 could influence or regulate the TE of target genes by modulating isoform production ratios (exon in- or exclusion), we estimated exon splicing rates by calculating the percentage spliced in (PSI) for all exons of known and correlating RBM20 target genes, as described previously (Schafer et al., 2015a). For PSI calculation, we re-mapped the 80 paired-end cardiac mRNA-seq ($2 \times 101\text{nt}$) datasets to improve splice site coverage using STAR v2.5.2b (Dobin et al., 2013), allowing a maximum of 6 mismatches.

Functional analysis of RBP associations and target genes

Known and predicted RBP-RBP interactions were retrieved from the STRING database (Szklarczyk et al., 2019) with confidence network edges and default settings. Moreover, we assigned biological functions to define gene targets with gProfiler2 v0.1.9 (archive revision fof4439, (Raudvere et al., 2019)) and extracted enriched sets of 'child' and 'parent' GO terms for the individual sets mRNA and TE targets ($p_{\text{adj}} \leq 0.05$).

Determination of frequencies and clustering of RBP binding sites

We searched for predicted dual-function RBP binding sites in the oRNAmnt database (Benoit Bouvrette et al. 2020). This database collects transcriptome-wide annotations of RBP target motifs which were defined through selection approaches; e.g. RNAcompete and RNA Bind-n-Seq (RBNS). We retrieved binding site coordinates across the full human transcriptome for three available dual-function RBPs: U2AF2, PUM1 and TRA2A. For each set of defined mRNA and TE targets, we calculated the frequency of binding sites (number of RBP motifs per kilobase) and the inter-site distances between neighbouring binding motifs to identify putative clusters of binding sites in UTR and CDS sequences. Intronic sequences were not included in this analysis.

Analysis of minimum free energy in 5' UTRs

We predicted 5' UTR secondary structures through energy minimization using RNAfold from the Vienna Package v2.4 (Lorenz et al. 2011). Using the 5' UTR sequence of each target gene as input, minimum free energies (MFE) were calculated and length-normalized to observe differences in UTR complexity for target genes that are positively or negatively correlating with RBPs.

General remarks on statistical analysis

Statistical analysis and generation of figures was done using R v3.6.2 (R Core Team (2020), 2020). A full list of tools and methods used for data analysis is stated in each corresponding Methods section. Statistical parameters such as n , median/mean, standard deviation (SD) and significance are named in the figures and/or the figure legends. The " p_{adj} " indicates the significance after correction for multiple testing using the Benjamini-Hochberg approach (Benjamini & Hochberg, 1995). The " n " represents the number of RBPs in Figure S3A.

TABLE AND FIGURE LEGENDS

Table S1: Analysis information for 143 RBPs Table with all 143 cardiac expressed RBPs, number of mRNA and TE correlating targets and significance of correlations, clusters of coregulated RBPs, and average RNA expression levels in human left ventricle.

Table S2: Dual-function RBPs Table with all 21 dual-function RBPs, number of target genes per molecular trait, and names and significance of the best 5 GO enrichment results.

Table S3: Dual-function RBPs' localization Table with all 21 dual-function RBPs and their cellular localization (0: absent; 1: present).

Figure S1. RNA-binding protein abundance predicts target translational regulation. (A) Bar plot displaying the patterns of expression of the 143 RBPs across tissues. Average expression values in transcript per million (TPM) units were retrieved from the Genotype-Tissue Expression (GTEx) Project (GTEx Consortium, 2013). Most of the RBPs are ubiquitously expressed across human tissues. (B) STRING protein-protein association networks (Szklarczyk et al., 2019) from six coregulated RBP clusters (see also Figure 1A). Most of the clustered RBPs are involved in known functional interactions. (C) Heatmaps with Glass' Δ scores for all 37 TE-RBPs quantifying the effect size of the witness effects for significant TE correlations.

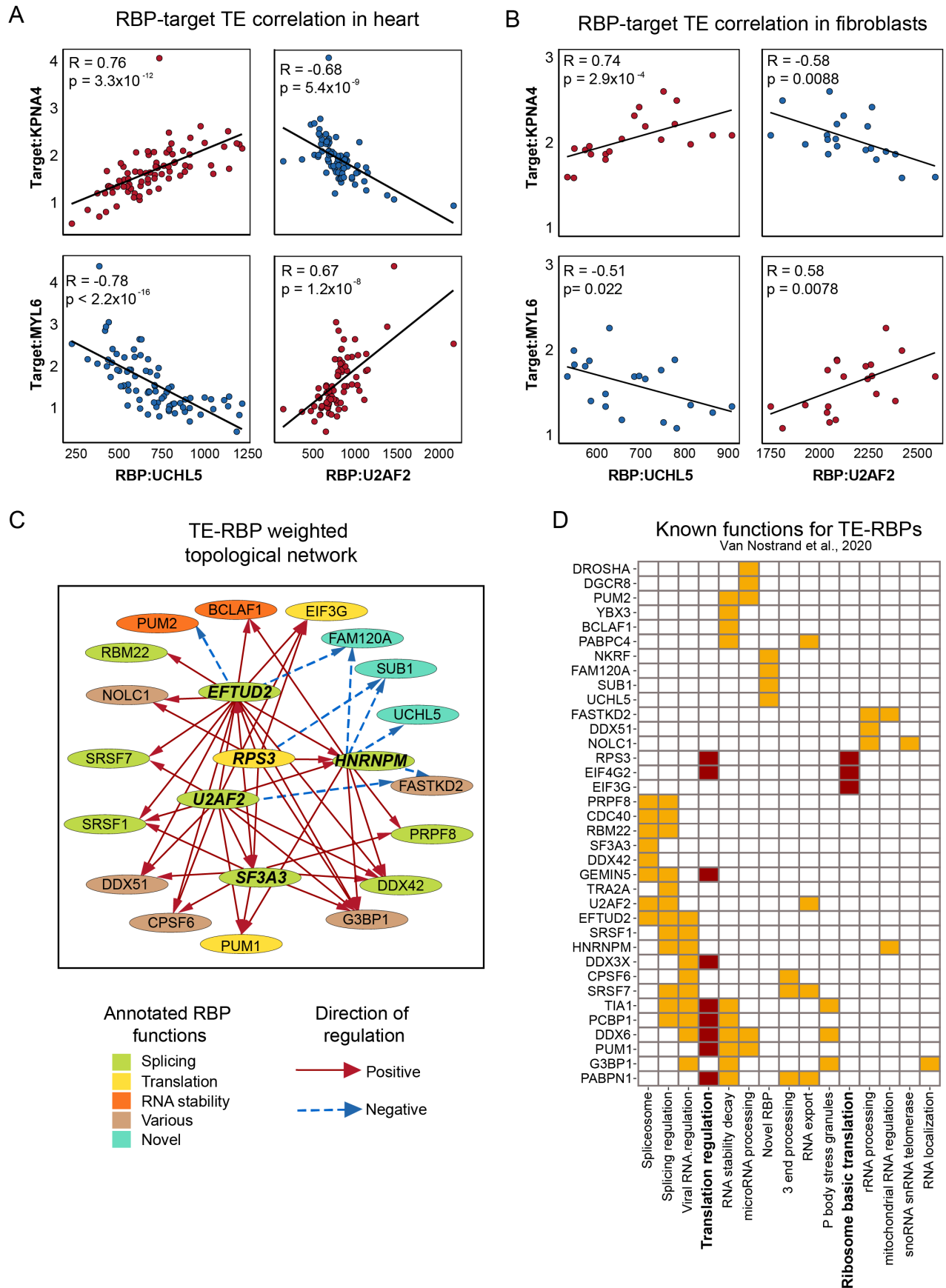


Figure S2. CLIP analysis identifies coregulated *in vivo* targets and novel master translational regulators in the human heart. **(A-B)** Scatter plots representing the correlation of heart **(A)** and primary cardiac fibroblasts **(B)** translational efficiencies between UCHL5 and U2AF2 and two shared targets, KPNA4 and MYL6. UCHL5 and U2AF2 have marked opposite effects on their shared targets, indicative of a competitive effect replicated in two independent datasets. Scores and level of significance of the two Spearman's correlations are displayed. **(C)** RBP-RBP network based on the weighted topological overlap (wTO) method (Gysi et al., 2018). Five central RBPs (EFTUD2, RPS3, U2AF2, HNRNPM, SF3A3) with robust correlation to target RBPs are highlighted. **(D)** Described functions by Van Nostrand and colleagues (Van Nostrand et al., 2020) for the set of TE-RBPs. Functions related to translation (translation regulation and ribosome basic translation) are highlighted with dark red boxes.

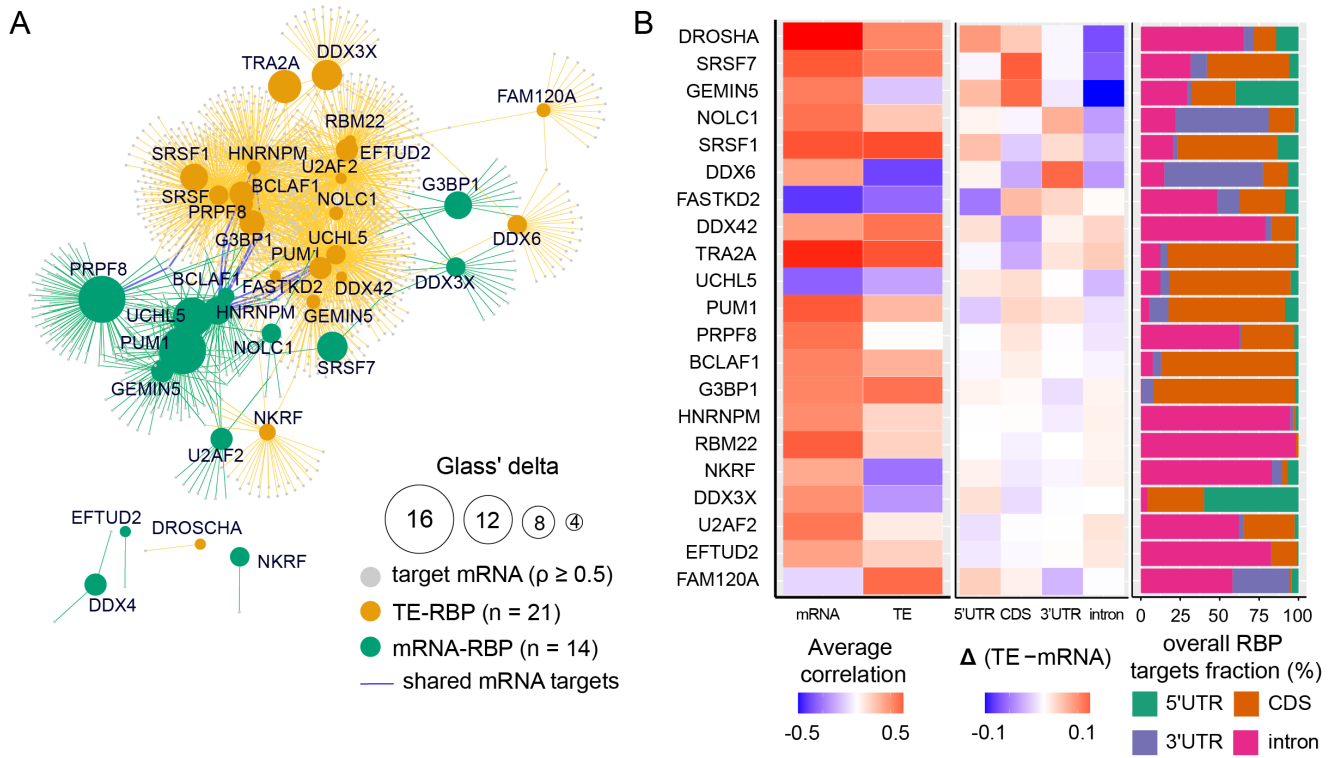


Figure S3. Dual-function RBPs regulate translation of distinct sets of target genes **(A)** Network representing dual-function RBP-target interactions for both mRNA-RBPs (green) and TE-RBPs (brown) of strong correlating pairs. Blue lines indicate shared targets in both mRNA abundance and TE regulation of the same RBP. **(B)** Left: heatmap representing the average mRNA and TE RBP-target correlation values for all 21 dual-function RBPs. Middle: heatmap representing differences in the relative proportion of feature binding sites (TE-mRNA) for all 21 dual-function RBPs. Right: bar plot showing the overall proportion of feature binding sites for all 21 dual-function RBPs. **(C)** Box plots with 5' UTR, CDS, and 3' UTR sequence lengths in nucleotides for mRNA and TE targets corresponding to the set of 21 dual-function RBPs. For each target gene, the most abundant isoform is represented.